Opuni et al., J Proteomics Bioinform 2017, 10:3
DOI: 10.4172/jpb.1000425

Journal of
Proteomics & Bioinformatics

Research Article Open Access

In silico Epitope Mapping of Glucose-6-Phosphate Isomerase: A Rheumatoid Arthritis Autoantigen

Opuni KFM[1#], Solomon S[2#], Metzen F[3], Frommholz D[3], Koy C[1], Röwer C[1], Glocker MO[1*], Illges H[2,3] and Anderson PC[4*]

[1]*Department for Proteome Research, Proteome Center Rostock, University of Rostock, Germany*
[2]*Department of Immunology, Department of Biology, University of Konstanz, Konstanz, Germany*
[3]*Department of Natural Sciences, Immunology and Cell Biology, University of Applied Sciences, Bonn, Germany*
[4]*Division of Physical Sciences, School of Science Technology Engineering and Mathematics, University of Washington, Bothell, USA*

Abstract

Rheumatoid arthritis-like symptoms can be initiated experimentally in naive K/BxN mice by simultaneously administering the two monoclonal antibodies 11H3 and 46H9. Both antibodies specifically recognize Glucose-6-Phosphate Isomerase (GPI), a known auto antigen in RA patients. Amino acid sequences of the Fv parts of the antibodies were determined by translating the respective hybridoma DNA sequences and served for three-dimensional structure modeling of the paratope regions. *In silico* docking of both Fv antibody structure models to the X-ray structures of the homodimeric murine GPI as well as to the homodimeric human GPI predicted the murine epitope of the 11H3 antibodies to comprise partial amino acid sequences QRVRSGDWKGYTGKS (aa134-148) and AAKDPSAVAK (aa232-241), generating an assembled (conformational) epitope. The 11H3 epitope on human GPI encompasses the matching partial amino acid sequences QRVRSGDWKGYTGKT (aa134-148) and AAKDPSAVAK (aa232-241). The epitope of the 46H9 antibody was determined to consist of the partial murine GPI amino acid sequence RKELQAAGKSPEDLEK (aa446-461) and the human GPI amino acid sequence RKELQAAGKSPEDLER (aa446-461), respectively, resembling consecutive (linear) epitopes. The predicted epitopes were verified by mass spectrometric epitope mapping using synthetic epitope peptides. Peptide QRVRSGDWKGYTGKS[GSMSGS] AAKDPSAAK included a small spacer sequence in between the epitope sequences, mimicking the assembled epitope for the 11H3 antibody. The peptide RKELQAAGKSPEDLEK represented the consecutive epitope for the 46H9 antibody. The determined B-cell epitopes of GPI and their interactions with the monoclonal antibodies provide a detailed structural understanding of immunological disease onset mechanisms in a mouse model of rheumatoid arthritis.

Keywords: *In silico* epitope prediction; Molecular dynamics; Docking; Epitope mapping: Epitope extraction; Mass spectrometry

Abbreviations: ASA: Accessible Surface Area; BrCN: Cyanogen Bromide; BSA: Buried Surface Area; CDR: Complementarity Determining Region; CO_2: Carbon Dioxide; DNA: Deoxyribonucleic Acid; FcR: Fragment Crystallizable Receptor; FCS: Fetal Calf Serum; Fv: Fragment Variable; GPI: Glucose-6-hosphate Isomerase; GST: Glutathione S-transferase; HT: Hypoxanthine-Thymidine; HAT: Hypoxanthine-Aminopterin-Thymidine; IgG: Immunoglobulin G; MD: Molecular Dynamics; PBS: Phosphate Buffered Saline; PCR: Polymerase Chain Reaction; PEG: Polyethylene Glycol; RA: Rheumatoid Arthritis; RMSD: Root Mean Squared Deviation; RMSF: Root Mean Squared Fluctuation; RNA: Ribonucleic Acid; RT: Room Temperature; SFM: Serum-free Medium; TRIS: Tris(hydroxymethyl)-aminomethane

Introduction

Rheumatoid Arthritis (RA) is a chronic inflammatory autoimmune disease affecting about 1% of the human population and is associated with inflammation and destruction of distal joints [1,2]. The etiology is unclear; however, genetic susceptibility, environmental influences, and microbial infections have been implicated in causing the disease [3]. Glucose-6-Phosphate Isomerase (GPI) is one of the autoantigens against which RA patients develop autoantibodies that have been found to circulate in serum and in synovial fluid of these patients [4-6]. The major histological characteristics of human RA, such as leukocyte invasion, synovitis, pannus formation, and cartilage and bone destruction have been observed in the K/BxN mouse model as well [7]. In addition, the K/BxN mouse disease shares other immunological abnormalities with human RA including cytokine imbalances, B-cell activation, and autoantibody production [8,9]. Like in humans, GPI was found deposited on the cartilage surface of normal mice, and also in high quantities of arthritic mice [10]. Purified GPI polyclonal IgG antibodies localize specifically to distal joints within minutes after intravenous injection and remain localized for at least 24 h [11]. Of note, arthritis-like symptoms were observed to develop in naive Balb/c mice by the transfer of polyclonal GPI antibodies or by transferring at least two different monoclonal GPI-specific antibodies [11,12]. In the K/BxN mouse, disease onset can be triggered by simultaneously administering the two pathogenic GPI-specific monoclonal antibodies 11H3 and 46H9 [13]. GPI-antibody complexes on joint cartilage surfaces have been shown to initiate an inflammatory cascade through the alternative complement pathway [10].

***Corresponding author:** Glocker MO, Director, Department for Proteome Research, Proteome Center Rostock, Institute of Immunology, University Rostock Medical Center and Natural Science Faculty, University of Rostock, Germany, Tel: +49-381-494-4930; Fax: +49-381-494-4932; E-mail: michael.glocker@med.uni-rostock.de

Anderson PC, Professor, Division of Physical Sciences, School of Science, Technology, Engineering and Mathematics, Office: Discovery Hall, 352-H, University of Washington, Bothell, USA, Tel: +1-425-352-3281; E-mail: pca4@uw.edu

#both authors contributed equally to this manuscript

Received February 21, 2017; **Accepted** March 09, 2017; **Published** March 15, 2017

Citation: Opuni KFM, Solomon S, Metzen F, Frommholz D, Koy C, et al. (2017) *In silico* Epitope Mapping of Glucose-6-Phosphate Isomerase: A Rheumatoid Arthritis Autoantigen. J Proteomics Bioinform 10: 60-72. doi: 10.4172/jpb.1000425

Correctly predicting an antibody's B-cell epitope is essential for many aspects of immunological understanding and clinical applications, including elucidating the molecular basis of immunity and autoimmunity, designing immunogens that stimulate antibody production for vaccine and therapeutic development [14,15], predicting cross-reactivity [15], and designing immunodiagnostic agents [16]. Subsequently, it is relevant to determine autoantigen-autoantibody interactions at the molecular level, and particularly to identify the epitopes to which the GPI-specific monoclonal antibodies 11H3 and 46H9 bind on either murine GPI or human GPI.

Epitope mapping is the process of identifying individual amino acid residues of the (auto)antigen involved in binding with the amino acid residues of the (auto)antibody paratope [17]. Epitope mapping approaches can be broadly classified as either structural (X-ray crystallography, nuclear magnetic resonance, and electron microscopy) or functional (competition assays, antigen modification, antigen fragmentation and synthetic peptides) [18]. Many of the functional approaches are performed in conjunction with mass spectrometry (recently reviewed in Opuni et al. [19]), and the most commonly used mass spectrometry-based epitope mapping approaches are epitope excision [20] and epitope extraction [21]. However, most of the experimental epitope mapping approaches are costly, time-consuming, and sometimes not viable since some antigens are insoluble in non-denaturing buffer solutions. Hence, *in silico* epitope prediction is a potentially useful alternative for epitope characterization on (auto) antigens towards specific (auto) antibodies [22,23].

Numerous computational tools have shown promise for reliable epitope prediction and have been reviewed extensively [16,24-32]. Among this list of computational tools, Molecular Dynamics (MD) simulations are particularly useful for structure-based epitope prediction that exploits not only static tertiary structural information about the relevant antibody and antigen, but also the time-dependent dynamical and conformational properties of both proteins and their predicted thermodynamic interaction energies. Consequently, MD simulations have been widely used for predicting B-cell epitopes [33-35]. Given the strengths and limitations of experimental methods and computational methods, in the present study we combine mass spectrometry and MD simulations in order to predict epitope regions of glucose-6-phosphate isomerase. We applied a set of *in silico* methods, including molecular modeling, docking, and MD simulations of X-ray structures of the autoantigens and of modeled Fv structures of the monoclonal antibodies 11H3 and 46H9. The predicted epitopes were confirmed experimentally by mass spectrometric epitope extraction using chemically synthesized epitope peptides.

Materials and Methods

Generation of GPI specific monoclonal antibodies 11H3 and 46H9

Mice were from own breeding at the animal center of the University of Konstanz where they were kept by veterinaries and with allowance from the authorities (Regierungspräsidium Freiburg). At the time of hybridoma generation extraction of organs from mice was done upon legal notification to the Regierungspräsidium Freiburg (formal notice, register no.: O-00/24). Formal allowance was not required as was confirmed by official notice (formal waiver of ethical approval, file number: 35-9185.5/414). The number of sacrificed mice was five. They were killed by cervical dislocation.

For the production of GPI specific monoclonal antibodies, one week prior to fusion SP2/0 myeloma fusion partner cells were expanded in Iscoves medium with 10% FCS. 96-well plates were plated with peritoneal cells obtained from C57BL/6 mice and the K/BxN mice were immunized with purified recombinant GPI after removal of Glutathione S-transferase (GST) tag. The recombinant GPI was expressed and purified as previously described [36]. On day of fusion, mice were sacrificed; spleens were harvested and teased to obtain single cell suspensions. Debris was removed by passage through a fine steel mesh, and washed cells were suspended in serum-free Iscoves media. The spleen cells were mixed in a 1:1 ratio with SP2/0 cells in 50 mL conical centrifuge tubes, pelleted at 500 g and the supernatants were discarded. Cell fusion was performed in a laminar hood with the cell pellets in a water bath at 37°C. To each cell suspension 1 mL pre-warmed 50% PEG solution was added drop-by-drop over 1 min while stirring after each drop. This process was repeated with an additional 1 mL of pre-warmed serum-free Iscoves medium. A further 7 mL of pre-warmed serum free Iscoves medium was added drop-by-drop over 2-3 min. The fusion mixes were pelleted at 500 g for 5 min at RT and the supernatants were discarded. Placing the cell pellets at 37°C, 10 mL of pre-warmed Iscoves medium with 20% FCS was forcibly added to disrupt the cell pellets and the volumes were adjusted to reach final cell densities of 2.5×10^6 cells/mL. Cell suspensions were then gently pipetted out at 100-125 cells/well into 96-well flat bottom plates with feeder cells and incubated in 5% carbon dioxide (CO_2) at 37°C. On days 2, 3, 4, 5, 7, 9, and 11, half the volumes of each well were aspirated using sterile Pasteur pipettes attached to a vacuum pump and 2 drops of Iscoves medium with 20% FCS and 1x HAT (hypoxanthine-aminopterin-thymidine), each, were added. On day 14 the feeding was done with Iscoves medium with 20% FCS and 1x HT (hypoxanthine-thymidine). From day 15 onward, the cells were fed with Iscoves medium with 20% FCS. The hybridomas were screened when the cells showed 10-25% confluence. About 100 µL supernatant from each well were removed and tested for GPI reactivity by GPI ELISA as previously described [36].

Next, limiting dilution cloning of hybridomas and adaption to serum-free media was performed. Briefly, 10 days prior to cloning, 96-well plates were plated with peritoneal cells obtained from C57BL/6 mice and grown at 37°C. On the day of cloning, hybridoma cells were counted and examined for viability by trypan blue dye exclusion stain. The viability was at least 80% for successful cloning. For each hybridoma, the cells were serially diluted in Iscoves medium with 20% FCS to give 4, 2, and 1 cells/mL. The diluted cells were then plated with 250 µL/well for each dilution in prepared 96-well plates. Cells were incubated at 37°C in 7.5% CO_2 for 5-7 days. The plates were microscopically examined for plating and cloning efficiency. Wells with single clones were analyzed for GPI reactivity using ELISA, and positive clones were expanded for freezing. The hybridomas were adapted to grow in serum-free media (SFM) to reduce protein loads in downstream processing. Hybridomas were grown in Iscoves medium with 10% FCS. The growing cells were then serially expanded in Iscoves medium with 10% FCS with 25% SFM followed by 50% SFM medium and finally in complete 100% SFM media.

DNA sequencing of GPI specific monoclonal antibodies 11H3 and 46H9

The total RNA extraction of 46H9 and 11H3 hybridoma cells was performed using the mi-Total RNA Isolation Kit (Metabion, Martinsried, Germany). cDNA synthesis was done using the Revert Aid First Stand cDNA Synthesis Kit (Thermo Scientific, Karlsruhe, Germany). For amplification of the V regions degenerated primers, binding to the leader sequences of the V regions and primers binding

to the constant region of IgG1 and kappa were used (primers and sequences are shown in Supplemental Table 1). For each hybridoma cell line ten PCR reactions were set up, six reactions for the amplification of light chain V regions and four reactions for the amplification of the heavy chain V regions. For each PCR reaction 2 µL from the cDNA synthesis reactions were used (PCR conditions for V region isolation are shown in Supplemental Table 2). Amplified DNA was extracted using the QIAquick Gel Extraction Kit (Qiagen, Hilden, Germany) and DNA ligation was performed using the InsTAclone PCR Cloning Kit (Thermo Scientific, Karlsruhe, Germany). The analysis of the recombinant clones was performed using colony PCR primers (Supplemental Table 3). For the colony PCR, white clones from the transformation were marked and tipped using a sterile pipette and re-suspended in PCR master mix containing 100 pmol of M13-forward and-reverse primer (Colony PCR conditions are shown in Supplemental Table 4).

Plasmids from bacterial colonies were isolated using the GeneElute HP Plasmid Miniprep kit (Sigma-Aldrich, München, Germany). Sequencing of V regions was done by gatc (http://www.gatc.org, Konstanz, Germany) using T7 primers. The sequences were characterized and analyzed using the Immunogenetics Database (http://imgt.org) [37].

Modeling of the 3D structures of the variable region fragments of GPI-specific monoclonal antibodies and atomic structure coordinates of Glucose-6-Phosphate Isomerase (GPI)

The amino acid sequences of the light chains and heavy chains of the variable region fragments (Fv) of the GPI-specific antibody 11H3, which had been translated from the DNA sequences, were used for modeling of the antibody structure. The antibody Fv structure was predicted using the freely available Rosetta Antibody server (http://rosie.rosettacommons.org/antibody) [38,39]. The "model H3 loop" option was selected. The server generated PDB files of 2048 candidate Fv structures and their energy values. The Fv structure of the GPI-specific antibody 11H3 possessing the minimum energy value was selected as our working structure. This procedure was also performed using amino acid sequences of the light chains and heavy chains of the variable region fragments (Fv) of the GPI-specific antibody 46H9, which had been translated from the DNA sequences. Fv structures were visualized using the UCSF Chimera (http://www.cgl.ucsf.edu/chimera/) molecular visualization software [40].

The coordinates of all non-hydrogen atoms of the dimeric structures of murine glucose-6-phosphate isomerase (PDB ID 2CVP) and of human glucose-6-phosphate isomerase (PDB ID 1IRI) were downloaded from the RCSB Protein Data Bank (www.rcsb.org).

Docking experiments between GPI and GPI-specific monoclonal antibodies, inter-epitope model comparison, and buried surface area (BSA) calculations

Docking experiments were performed for the murine GPI antigen-11H3 antibody pair using the Fv structure of 11H3 antibody and the X-ray structure of the murine GPI antigen in conjunction with the antibody-modeling feature of the ClusPro 2.0 server (http://cluspro.bu.edu/login.php) [41,42]. Next, the Chimera software was used to perform atom-to-atom contact analyses between murine GPI antigen and amino acids in the paratope region of 11H3 for all the docked murine GPI antigen-11H3 antibody structures using a contact distance of ≤4 Å. The amino acid sequence of the murine GPI that formed contacts with the 11H3 paratope region were considered as epitope models [17]. The above procedure was identically performed for the human GPI antigen-11H3 antibody pair, the murine GPI antigen-46H9 antibody pair, and the human GPI antigen-46H9 antibody pair.

An inter-epitope model comparison was performed for the 11H3 antibody docked to either murine or human GPI antigen. First, the amino acid sequence position of the predicted epitope of 11H3 antibody on murine GPI from all the epitope models of murine GPI antigen-11H3 antibody pair was compared with that of human GPI antigen-11H3 antibody pair. Next, amino acid residue similarity of the matching sequence position of epitope models from murine GPI antigen-11H3 antibody pair was compared with the respective epitope model from human GPI antigen-11H3 antibody pair. Epitope model pairs that shared both high sequence position and amino acid identity were considered as potential candidates for epitope identification. This procedure was identically performed for the 46H9 antibodies docked to either murine or human GPI.

The EpiMED-Surf bioinformatics tool [43] was used to calculate the Buried Surface Area (BSA) upon antibody binding to the murine GPI epitope surfaces for the docked antigen-antibody complex. The "calculate electrostatics" and "calculate hydrophobicity and ASA (accessible surface area)" options were selected. BSA was calculated by summing the atomic surface values of all atoms of the amino acid residues that were part of the predicted epitope region on murine GPI antigen docked to 11H3 antibody. BSAs were also calculated for the predicted epitope regions on murine GPI antigen docked to 46H9 antibody.

Molecular dynamics (MD) simulations of 3D structures of the immune complexes and clustering of MD simulations trajectory

The atomic coordinates of the docked structure for the murine GPI antigen-11H3 antibody pair were used for MD simulations using the GROMACS v. 4.6.7 software package [44], running on the Hyak cluster of computers at University of Washington, Seattle (http://www.engr.washington.edu/mycoe/computing/facultyresources.html) and on local computers. MD simulations were performed using the AMBER99-ILDN force field [45]. The initial structure was minimized in vacuo using a steepest-descent algorithm to relieve unfavorable contacts and was subsequently solvated in a dodecahedral box of TIP3P water molecules [46] such that a minimum distance of 1.0 nm was maintained between any protein atom and the edges of the box. System charge neutrality was maintained by assigning seven chloride ions to randomly selected positions in the box. The solvated system was then subjected to 5000 steps of steepest-descent energy minimization using cutoff values of 1.0 nm for electrostatic interactions and van der Waals interactions.

Equilibration of the system was next carried out by performing a 1.0-ns molecular dynamics simulation of the minimized solvated system in the NVT (constant number of particles, volume and temperature) ensemble in which the temperature was gradually raised from 200 K to 298 K (25°C) using the Berendsen thermostat [47]. Periodic boundary conditions were modeled using the Particle Mesh Ewald method [48], and cutoff values of 1.0 nm were used for electrostatic interactions and van der Waals interactions. Position restraints with a force constant of 1000 kJ/mol/nm^2 were placed on all non-hydrogen protein atoms, and covalent bonds were constrained using the LINCS algorithm [49]. A second equilibration simulation of length 1.0 ns was subsequently performed in the NPT (constant number of particles, pressure and temperature) ensemble at 298 K and at 1 atom pressure, applying the Berendsen coupling scheme. The final atomic velocities and positions

from the NVT trajectory were used as input. The same position restraints as used previously were applied to non-hydrogen protein atoms. A subsequent 5.0-ns simulation was performed at 298 K in the NPT ensemble in which no position restraints were applied.

Following equilibration, production molecular dynamics simulations were performed in triplicate for 50 ns each using different initial velocities in each simulation. This procedure was identically performed for the murine GPI antigen-46H9 antibody complex and for unbound murine GPI antigen using the previously generated structure of the murine GPI antigen-46H9 antibody complex and the murine GPI antigen crystal structure, respectively, as input structures.

Structures from equally spaced snapshots over the last 15 ns of all production molecular dynamics simulations trajectories for all modeled antigen-antibody complexes were clustered using the "g_cluster_mpi" utility of the GROMACS software. Clusters were assigned using (root mean squared deviation) RMSD cutoff of 0.1 nm as a metric.

Prediction of changes in binding energies of antigen-antibody complexes due to point mutations

The BeAtMuSiC web server (http://babylone.ulb.ac.be/beatmusic/query.php) [50] was used for predicting changes in binding energies of the docked murine GPI antigen-11H3 antibody complex upon introducing point mutations in the antigen-antibody binding interface. A representative structure of the most highly populated cluster from the MD trajectories of the murine GPI antigen-11H3 antibody complex served as the analysis structure. The murine GPI antigen and 11H3 antibody were selected as the two binding partners and the server automatically performed systematic mutations of interface residues. This procedure was likewise performed for the docked murine GPI antigen-46H9 antibody complex using a structure representative of the most highly populated cluster from the murine GPI antigen-46H9 antibody simulation trajectories.

Western blot analyses of full-length GPI antigens

Murine GST-GPI fusion protein solution (1.43 µL; 1.39 µg/µL) or human GPI protein solution (4.4 µL; 0.45 µg/µL) were incubated with SDS sample buffer (2.5 µL; 312.5 mM TRIS/HCl pH 6.8, 10% SDS, 4% bromophenol blue, 50% glycerol, 325 mM DTT) at 95°C for 5 min. Both mixtures were loaded onto a NuPAGE Novex 10% Bis-TRIS gel in separate pockets. 6 µL of the PageRuler Prestained Protein Ladder (Thermo Scientific, USA) was also loaded onto the gel and functioned as an apparent molecular mass standard. The gel was placed in an Xcell Surelock™ Minicell electrophoresis chamber. 500 mL of 3-(N-morpholino)propanesulfonic acid (MOPS) buffer (50 mM MOPS, 50 mM Tris, 3.5 mM SDS, 1.0 mM EDTA) was used as running buffer. The gel was allowed to run for 45 min at a constant voltage of 200 V. The separated protein bands were then blotted onto a PVDF membrane (Immobilon, Millipore, Schwalbach, Germany) for 60 min at a constant current of 1.2 mA/cm^2. The PVDF membrane was subsequently incubated with 10 mL blocking buffer (1:1 mixture of Odyssey blocking buffer (LI-COR, Nebraska, USA) and 10 mM PBS) for 60 min at RT. The membrane was incubated with the primary antibody, 11H3 monoclonal antibody, in 1:1000 dilutions (10 µL 11H3 monoclonal antibody in 10 mL blocking buffer/0.1% Tween 20) overnight in a cold dark room. The membrane was washed 4 times (5 min each) with 10 mL wash buffer (10 mM PBS, 0.1% Tween 20). The PDVF membrane was further incubated with the secondary antibody, IRDye 800 CW conjugated Goat Anti Mouse (LI-COR, Nebraska, USA), in 1:10,000 dilutions (1 µL IRDye 800CW conjugated Goat Anti Mouse in 10 mL blocking buffer/0.1% Tween 20) for 60 min at RT. The membrane was washed 4 times (5 min each) with 10 mL wash buffer and was rinsed with 10 mM PBS buffer afterwards. Detection was performed using an Odyssey Infrared Imaging System (LI-COR, Nebraska, USA). This procedure was applied with a second gel/blot using the 46H9 monoclonal antibody as the primary antibody with the following modifications: 1:1000 dilutions of the primary antibody and 1:50,000 dilution of the secondary antibody.

Epitope extraction

The peptide with amino acid sequence QRVRSGDWKGYTGKS[GSMSGS]AAKDPSAK to mimic the 11H3 antibody epitope and the peptide RKELQAAGKSPEDLEK of the 46H9 antibody epitope were obtained as lyophilized powders (Peptides and Elephants GmbH, Potsdam, Germany). These peptides were dissolved in 10 mM PBS buffer, pH 7.4, with a final concentration of 500 µM and stored at -20°C. Peptide mixture I consisted of the 11H3 epitope peptide (315 pmol), human ACTH clip (18-39) (20 pmol; Sigma-Aldrich, Saint Louis, USA), and oxidized Insulin B chain (100 pmol; Sigma-Aldrich, Saint Louis, USA), dissolved in 50 µL of 10 mM PBS buffer, pH 7.4. Peptide mixture II was prepared from 20 pmol of the 46H9 epitope peptide and peptide standard (2 pmol, consisting of Angiotensin II, Angiotensin I, Substance P, Bombesin, ACTH clip (18-39), Bruker Daltonik, Bremen, Germany); dissolved in 50 µL 10 mM PBS buffer 7.4.

Epitope extraction [51] was performed using a programmable Rainin E4 XLS eight-channel electronic pipette (Mettler Toledo, Germany), equipped with 200 µL Pure Speed Protein Tips that contained 5 µL of protein G resin (Mettler Toledo, Germany). Equilibration of the Pure Speed Protein Tips was done with 100 µL equilibration buffer (100 mM sodium dihydrogen phosphate, 140 mM sodium chloride, pH 7.5). Then, 50 µL of 0.63 pmol/µL 11H3 monoclonal antibody (32 pmol) was applied in one tip and the GPI-specific 46H9 monoclonal antibody (50 µL of 0.2 pmol/µL) was applied in a second tip as a control in parallel. For immobilization of the antibodies on the protein G resins antibody solutions were aspirated and dispensed in six cycles for 15 min. Next, excess of unbound antibodies was removed by washing with 50 µL of 10 mM PBS buffer using six cycles of aspiration/dispension for 10 min. 50 µL of peptide mixture I (see above) was allowed to interact with the immobilized antibodies for 60 min using six cycles of aspiration/dispension, each. Non-specifically bound peptides were sequentially washed-off using four washing steps (three aspiration/dispension cycles each) with 100 µL each of wash buffer 1 (10 mM sodium dihydrogen phosphate, 140 mM sodium chloride in water, pH 7.5), wash buffer 2 (140 mM sodium chloride in water, pH 7.0), wash buffer 3 (14 mM sodium chloride in water, pH 7.0), and wash buffer 4 (0.3 mM TRIS/HCl, 0.25 mM n-octyl-β-D-glucopyranoside), respectively. The still bound (epitope) peptides were then eluted with 20 µL of elution buffer (3 mM hydrochloric acid, pH 2.0). The eluted peptides were subjected to MALDI-ToF MS analysis. The above procedure was also used for epitope mapping of 46H9 antibody with the following adjustments: 200 µL Pure Speed Protein Tips that contained 5 µL of protein A resin; 50 µL each of GPI-specific 46H9 monoclonal antibody (0.2 pmol/µL) was applied in one tip and GPI-specific 11H3 monoclonal antibody (0.63 pmol/µL) was applied in parallel in a second tip as a control; and 50 µL of peptide mixture II (see above) was allowed to interact with the immobilized antibodies for 60 min using six cycles of aspiration/dispension, each.

MALDI-ToF MS analysis

The epitope peptide containing solutions from the epitope

extraction experiments (10 µL each) were desalted using ZipTip C18 tips (Millipore, Billerica, USA) according to the manufacturer´s instructions [51]. The eluted samples (0.5 µL, each) were spotted onto an AnchorChip™ 600/384 target plate (Bruker Daltonik, Bremen, Germany). 2.0 µL of 2,5-dihydroxybenzoic acid (DHB, LaserBio Labs, France) matrix solution (5 mg DHB dissolved in 1000 µL of 50% acetonitrile (ACN)/0.1% TFA)) was added and mixed on the target. Spots were air dried at room temperature. The target was then inserted into the SCOUT source of the Reflex III MALDI-ToF MS instrument (Bruker Daltonik) [52]. Measurements were performed with the following instrumental settings; nitrogen laser wavelength, 337 nm; nitrogen laser pulse width, 3-5 ns; reflector mode acceleration voltage, 23.0 kV. Data acquisition was performed using positive ion reflector mode (~100 shots per spectrum) in the mass range of m/z 1000-4000. The instrument was calibrated externally using a standard peptide mixture [53]. Data were acquired and processed using the FlexAnalysis 2.4 and BioTools 3.0 programs (Bruker Daltonik).

Results

Modeling of 3D structures of the Fv parts of monoclonal anti-GPI antibodies

Our *in silico* epitope prediction started with generating 3D structures of the Fv part of the 11H3 mono-clonal antibody using amino acid sequences of the variable regions of the heavy and light chains, respectively (Supplemental Figure 1).

Amino acid sequences were obtained by translation of the hybridoma DNA sequences. The Complementarity Determining Region (CDR) H3 was modeled de novo while comparative modeling was used for the canonical conformations of the other CDRs. Proper orientation of V_L-V_H rigid-body and CDR backbone as well as side-chain conformation was ensured by energy minimization using a 50-cycle Monte Carlo minimization procedure [54].

The secondary structure elements of the Fv structure were antiparallel β-strands as structural scaffolds and loops in which the CDRs were located. The latter were assigned using the Chothia rule [55]. This procedure was identically performed to generate the three-dimensional 46H9 antibody Fv structure (Supplemental Figure 1). Detailed antibody server modeling parameters have been published [39,56]. Only the Fv structure with the lowest energy was used for the docking analysis since it represents the most native state of the predicted structure.

Prediction of GPI epitopes by *in silico* molecular docking

For modeling the interaction site of the complex consisting of the murine GPI antigen and the 11H3 monoclonal antibody, we used the PDB file for the antigen (PDB ID: 2CVP) as well as that for the antibody Fv part (see above) and subjected them to rigid body *in silico* docking using the ClusPro 2.0 server. The docking was performed using the antibody mode of the ClusPro 2.0 server, which is based on asymmetric statistical potentials [57]. Twenty-nine murine GPI-11H3 antibody complex structures were generated, together with their weighted scores by which they were ranked. The first ten murine GPI-11H3 antibody complex structures were shortlisted and the amino acid residues of the murine GPI antigen that made contact with the paratope amino acid residues of the 11H3 antibodies were considered as epitope models (Table 1).

All epitope models consisted of mainly continuous stretches of partial amino acid sequences. In epitope model 10, the partial sequence ^{417}RKGL^{420} was flanked with residues from somewhat more distant sequence positions (e.g. ^{423}K). These residues were located on one and the same of the two murine GPI chains (in this example on chain A from the homodimer). Almost all suggested epitope models also included parts from the other chain of the murine GPI homodimer. In epitope model 10, for instance, the participating amino acid residues on the B chain of murine GPI were ^{227}E ^{529}LEGSS ^{550}K ^{553}RD ^{556}K. Since the GPI antigen is a homodimer, antibody binding was in three cases mirrored on "inverse" chains. Epitope models 10 and 11, for example,

Epitope model	Chain	Epitope motif[a]	SA [Å²][b]
10	A	^{417}RKGL ^{423}K	415.21
	B	^{227}E ^{529}LEGSS ^{550}K ^{553}RD ^{556}K	886.15
11	A	^{527}PE ^{530}EGSSA ^{536}T ^{550}K ^{553}RD ^{556}K	1087.83
	B	^{417}RKGL ^{423}K	402.94
12	A	^{89}K ^{92}YTEDR ^{114}DGK ^{366}K ^{513}W	900.72
	B	^{446}R ^{450}QAAGKSPEDLEKL	1206.94
13	A	^{448}E ^{450}QA ^{453}GKS ^{458}D ^{461}KL	723.64
	B	^{89}K ^{93}TEDR ^{114}DGK ^{211}KT ^{214}T ^{216}Q ^{248}TNT ^{252}K ^{255}E ^{267}WD ^{519}KQ ^{524}K	1787.02
14	A	-	-
	B	**^{134}QR ^{140}D ^{142}KGYTGK ^{202}E ^{232}AAKDPSA ^{241}K ^{254}K**	1377.97
15	A	^{134}QR ^{138}S ^{140}DWKGYTGKS ^{237}S ^{240}AK ^{261}Q	1171.33
	B	-	-
16	A	^{135}R ^{141}WK ^{144}YTG ^{234}KDPSA ^{241}K ^{254}K ^{259}D ^{261}Q	1248.04
	B	-	-
17	A	^{130}K ^{134}QR ^{137}RSGD ^{142}K ^{145}TGKS ^{176}KGG ^{180}R ^{291}D	1419.87
	B	^{197}A	87.24
18	A	^{89}K ^{95}D ^{114}D ^{116}K ^{212}T ^{214}T ^{249}N ^{251}AK ^{520}Q ^{524}K	953.27
	B	^{448}E ^{450}QAAGKS ^{457}ED ^{466}K	770.32
19	A	^{112}KVDGKDV ^{120}PE ^{124}R ^{248}T ^{250}TA ^{254}K ^{265}EFW	1225.91
	B	-	-

[a]Distance between epitope and paratope amino acid groups ≤4 Å
[b]SA: Surface Area

Table 1: Suggested epitope motifs on the murine GPI dimer towards the paratope region of the 11H3 monoclonal antibody.

are such "mirrored models" with high similarities to each other. Each of the ten top-ranking epitope models provided accessible surfaces larger than 1100 Å^2, which is more than the average epitope surface of 650–1000 Å^2 [58]. For the antigen-antibody complex consisting of the human GPI antigen and the 11H3 antibodies, the first ten epitope model predictions were likewise grouped after independent molecular docking (Supplemental Table 5).

In some of the epitope models of human GPI, the complete amino acid sequence was contributed by only one chain of the GPI dimer. The amino acid residues ^{134}QR ^{138}SGDWKGYTGKT ^{237}S ^{240}AK ^{261}Q of epitope model 26, for instance, were located only on the A chain. "Mirror pairs" with human GPI are epitope models 20 and 21, 22 and 23, as well as 24 and 25. These "mirror pairs" have identical sequence positions and amino acid residues.

As sequence homology between murine GPI and human GPI is approximately 89% and because both antibodies recognized both antigens in denatured form in a comparable fashion (Western blot data shown in Supplemental Figure 2), an inter-epitope species comparison was performed to identify those epitope models with best sequence similarities between the two species.

For example, the epitope model group that contained epitope models 10 and 11 from the murine GPI-11H3 antibody pair matched closely with the sequence positions from the epitope model group that encompassed epitope models 20 and 21 from the human GPI-11H3 antibody pair. However, although the sequence positions in these cases were nearly identical, the respective amino acids at a given sequence position were not. By contrast, epitope model 14 from the murine GPI-11H3 antibody pair exhibited nearly identical amino acid positions and nearly identical amino acid residues as did epitope model 26 from the human GPI-11H3 antibody pair. In both cases, the predicted epitope sequences were found on one and the same GPI amino acid chain without any contribution of the other chain of the GPI dimer. Consequently, epitope model 14 (bold print in Table 1) from the murine GPI-11H3 pair and epitope model 26 (bold print in Supplemental Table 5) from the human GPI-11H3 pair were considered as best potential epitope candidates.

Docking calculations and sequence similarity analyses were performed identically for the complexes that consisted of the 46H9 antibody Fv part bound to either the murine GPI or the human GPI dimer (Table 2 and Table S6). Here, epitope model 36 (bold print in Table 2) from the murine GPI-46H9 pair and epitope model 44 (bold print in Supplemental Table 6) from the human GPI-46H9 pair were considered best equivalents to each other, and hence, best epitope candidates. They provided similar consecutive sequence lengths and nearly identical amino acid sequences.

The best epitope models for either of the two monoclonal antibodies were visualized on the 3D structure of the GPI homodimer with epitope model 4 and 26, respectively, for 11H3 and epitope model 36 and 44, respectively, for 46H9 on either the murine GPI or the human GPI dimer (Figure 1). The visualized epitope model (partial sequences of model 14 in Table 1) of the 11H3 monoclonal antibody comprises aa134-148 (QRVRSGDWKGYTGKS) and aa232-241 (AAKDPSAVAK) on murine GPI, consisting of a helix-loop-helix motif that provides an assembled (conformational) epitope.

It should be noted that from all complexes of the murine GPI-11H3 pair, epitope models 14, 15, 16, and 17 were located at nearly identical molecular surface regions (marked in blue in Figure 1) and epitope models 10, 11, 12, 13, 18, and 19 were located on different surface regions of the murine GPI dimer. Interestingly, all human GPI-11H3 antibody complexes showed the 11H3 Fv component docked to one and the same surface region around the predicted epitope model (marked in blue in Figure 1) with only subtle differences.

Comparably, the best epitope model of the 46H9 monoclonal antibody (partial sequence of epitope model 36 in Table 2), is located on the molecular surface of murine GPI comprising aa446-461 (RKELQAAGKSPEDLEK), hence a consecutive (linear) epitope. All the murine GPI-46H9 complexes and all the human GPI-46H9 complexes showed the 11H3 Fv component for all the 10 epitope models, each attached to one and the same surface region around the

Epitope model	Chain	Epitope motif[a]	SA [Å^2][b]
30	A	^{27}R ^{30}FEADP ^{438}K ^{441}L ^{444}E ^{447}K	841.78
	B	^{524}K ^{528}E ^{534}A ^{536}TSHDS ^{543}N	551.12
31	A	^{524}K ^{536}TSHDS ^{543}N	427.35
	B	^{16}W ^{20}N ^{23}N ^{25}K ^{27}REL ^{31}EADPER ^{60}VSKE ^{438}K ^{441}L ^{443}EE ^{447}K	1631.42
32	A	^{176}K ^{411}Q ^{413}QHPIRKG ^{481}K	784.46
	B	^{216}Q ^{223}E ^{226}KE ^{230}LE ^{234}K ^{252}K ^{255}E ^{523}K ^{526}EP ^{530}EGSS ^{550}KQ ^{553}RD ^{556}K	1995.86
33	A	^{216}Q ^{223}E ^{226}KE ^{230}LE ^{234}K ^{252}K ^{254}KE ^{523}K ^{526}EP ^{530}EGSS ^{553}RDTK	1904.15
	B	^{176}K ^{414}HPIRKGL ^{424}I	709.30
34	A	^{555}TKL	341.17
	B	^{45}NTNH ^{106}RSNT ^{123}N ^{174}Y ^{176}K ^{291}DH ^{294}EQ ^{298}SG ^{302}W ^{305}QH ^{309}K ^{485}F	1536.83
35	A	^{48}H ^{106}R ^{108}N ^{127}D ^{130}K ^{134}Q ^{137}RS ^{173}PYSK ^{288}VG ^{291}DH ^{294}EQ ^{414}H ^{481}K ^{483}T	1371.74
	B	^{556}KL	298.12
36	A	^{89}K ^{95}D ^{114}DG ^{366}K	478.89
	B	**^{450}Q ^{453}GKSPED ^{460}EK**	891.02
37	A	^{1}MAA ^{6}R ^{73}KSRG ^{83}N ^{89}K ^{95}D ^{114}D ^{365}TKSGAR	1334.61
	B	^{446}R ^{454}KSPED ^{460}EK ^{464}P	869.46
38	A	^{536}T ^{539}DS	166.92
	B	^{20}N ^{23}N ^{25}K ^{27}RELFEADPER ^{39}N ^{62}KE ^{66}Q ^{443}E ^{447}K	1674.28
39	A	-	-
	B	^{73}KSRG ^{78}EAARDN ^{85}F ^{88}S ^{109}TP ^{112}K ^{305}Q ^{308}LKTPL ^{366}K ^{506}D	1415.58

[a]Distance between epitope and paratope amino acid groups ≤4 Å
[b]SA: Surface Area

Table 2: Suggested epitope motifs on the murine GPI dimer towards the paratope region of the 46H9 monoclonal antibody.

predicted epitope model (marked in red in Figure 1). Details of the predicted epitope-paratope interactions such as hydrogen bonding, salt bridges, ionic, cation-π, and hydrophobic [59-61] interactions have been summarized (Supplemental Tables 7-22).

Most importantly, the predicted epitope models of the 11H3 and 46H9 monoclonal antibodies are located distant from each other and do not share any surface regions (or partial sequences) on either murine GPI or human GPI. This observation is explained by the substantial differences in the amino acid sequences of the CDR regions, creating two completely different paratopes on the respective monoclonal antibodies.

Conformational mobility characterization of the epitope regions of the antibody-antigen complexes

According to the RMSD plot of the MD simulation trajectories of murine GPI antigen complexed with either monoclonal antibody 11H3 or 46H9, the simulated antigen-antibody systems remained unchanged in both cases after 27 ns (data not shown). Hence, the last 15 ns of the 50 ns MD simulation trajectories were used for the calculation of positional flexibilities of backbone atoms of the murine GPI antigen in terms of alpha carbon root mean squared fluctuation (RMSF) as a function of amino acid position in the murine GPI sequence. The RMSF plot for murine GPI bound to the 11H3 antibody (epitope model 14; dotted line in Figure 2) showed in general slightly higher flexibility as compared to the unbound murine GPI antigen (solid line). Most interestingly, upon antibody binding there was a slight decrease in flexibility at the amino acid regions aa130-150 and aa225-245, both of which are part of the predicted epitope model 14. This result stands in agreement with a reduction in conformational mobility of the amino acid residues of the epitope regions upon interaction with the paratope of the 11H3 antibody. By contrast, the slight decrease in flexibility at the N-terminal end upon antibody binding may simply be an artifact, as flexibility estimations of N-terminal and C-terminal tail regions are typically prone to erroneous outcomes.

Both RMSF plots of (i) murine GPI bound to the 46H9 antibody (epitope model 36; dotted line in Figure 3) and (ii) the unbound murine GPI (solid line) likewise showed regions of high and low flexibilities. Of note, the RMSF curve of bound murine GPI showed an offset towards higher flexibility as compared to the unbound murine GPI, since a different utility of the GROMACS software was used. Despite this offset, there was a significant decrease in flexibility at the amino acid region aa440-470, which encompassed the sequential epitope model 36, again indicating reduction in conformational mobility of the epitope region upon interaction with the paratope of the 46H9 antibody.

Estimation of key amino acid residues within the predicted epitopes

To estimate which of the amino acid residues of epitope model 14 may play key roles in 11H3 antibody binding, relative binding energy changes between the murine GPI antigen and the 11H3 antibody upon site-specific exchanges of amino acid residues from the predicted epitope sequence were determined. The wild-type amino acid residues in the epitope model 14 sequence were assigned as reference ($\Delta G_{bind}=0$). Amino acid residues different from the wild-type amino acid residue at a given position on the epitope sequence with higher binding energies, i.e., positive $\Delta\Delta G_{bind}$ values, were considered as having a destabilizing effect on the epitope-paratope interaction. By contrast, amino acid residues with negative $\Delta\Delta G_{bind}$ values were considered as providing a stabilizing effect on the epitope-paratope interaction (Figure 4I).

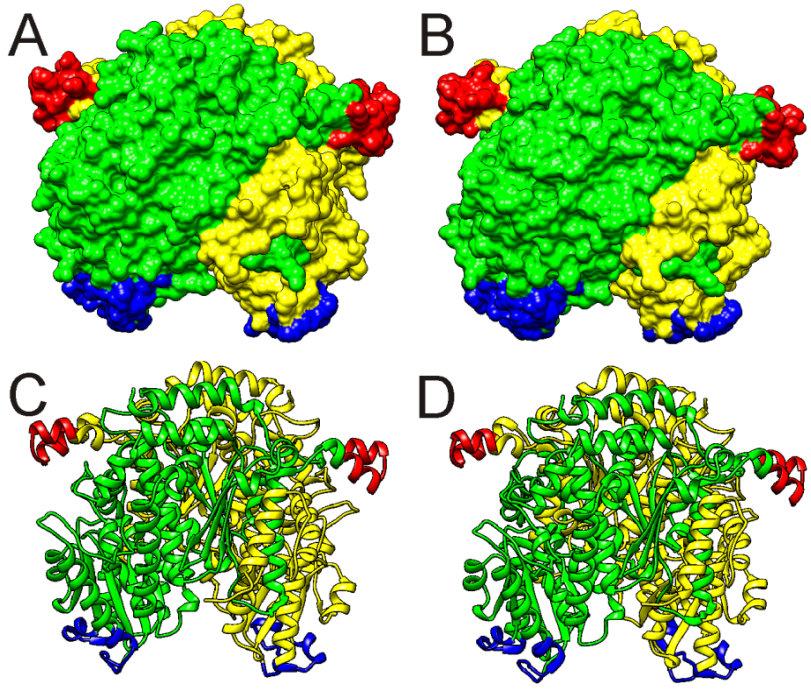

Figure 1: Three-dimensional structures of GPI homodimers. A and C: Murine GPI (PDB ID 2CVP). B and D: Human GPI (PDB ID 1IRI). A and B: Molecular surfaces. Spheres indicate van-der-Waals radii of surface atoms. C and D: Cartoon views. Ribbons indicate locations of backbone atoms. The monomers are shown in green (A chain) and yellow (B chain). Blue: epitope region for monoclonal antibody 11H3. Red: Epitope region for monoclonal antibody 46H9.

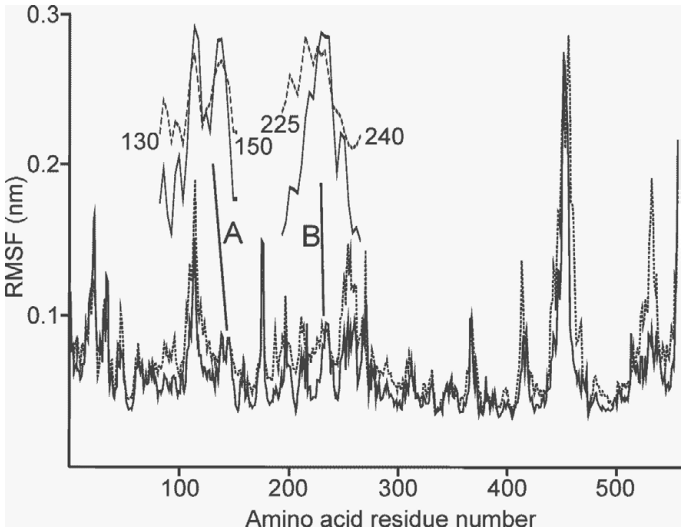

Figure 2: Positional flexibilities of backbone atoms of murine GPI (root mean squared fluctuation, RMSF) as a function of amino acid position in the amino acid sequence. Solid line: Unbound murine GPI. Dotted line: Murine GPI bound to antibody 11H3. A and B show zoomed regions around the partial sequences of the epitopes.

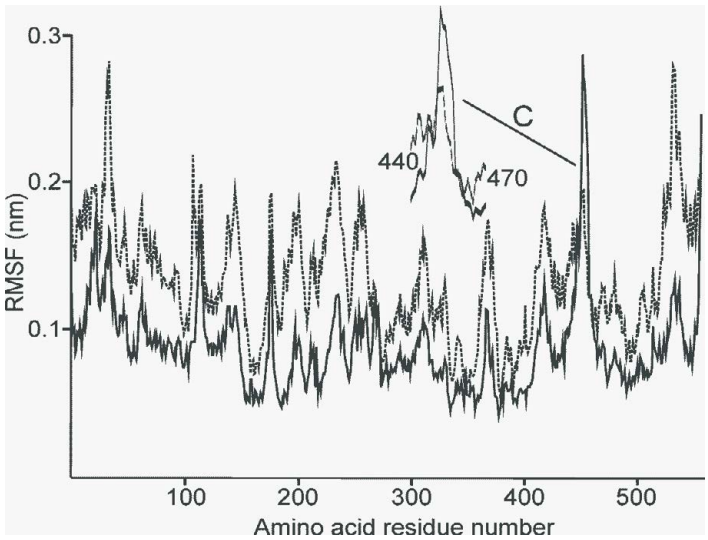

Figure 3: Positional flexibilities of backbone atoms of murine GPI (root mean squared fluctuation, RMSF) as a function of amino acid position in the amino acid sequence. Solid line: unbound murine GPI. Dotted line: Murine GPI bound to antibody 46H9. C shows a zoomed region around the partial sequence of the epitope.

In those cases when replacement of the wild-type amino acid residue by any other amino acid residue always yielded positive ΔΔGbind values (the respective column in Figure 4 starts above the "0" line), the respective wild-type amino acid residue (G146 on the left and K234, P236, and S237 on the right) was considered crucial for epitope-paratope interaction of the 11H3 antibody. The above analysis was identically performed for the murine GPI antigen complexed to the 46H9 antibody (epitope model 36). Here amino acid residues S455, P456, and E457 have been identified as important for binding the 46H9 antibody (Figure 4II).

Validation of *in silico* epitope predictions by experimental data

The epitope peptide of the GPI-specific monoclonal antibody 11H3 on the murine GPI antigen was confirmed by affinity mass spectrometry using peptide mixture I (Supplemental Table 23) that contained the 11H3 epitope peptide and two standard peptides as controls. MALDI-ToF MS analysis of peptide mixture I showed singly charged ion signals of the 11H3 epitope peptide and other standard peptides (Figure 5IA). The ion signal of the 11H3 epitope peptide was accompanied by an ion signal that indicated partial oxidation at the methionine residue.

Peptide mixture I was allowed to interact with the GPI-specific monoclonal antibody 11H3 as well as with the monoclonal antibody 46H9, which served as a non-specific control. MALDI-ToF MS analysis of the eluted solutions showed the exclusive presence of an intense singly charged ion signal at m/z 3169.57 which corresponds to the 11H3 epitope peptide when peptide mixture I was exposed to 11H3 (Figure 5IB). Again an ion signal of the oxidized peptide was present, indicating that the methionine residue was not involved in antibody binding. By contrast, MALDI-ToF MS analysis of the eluted solution

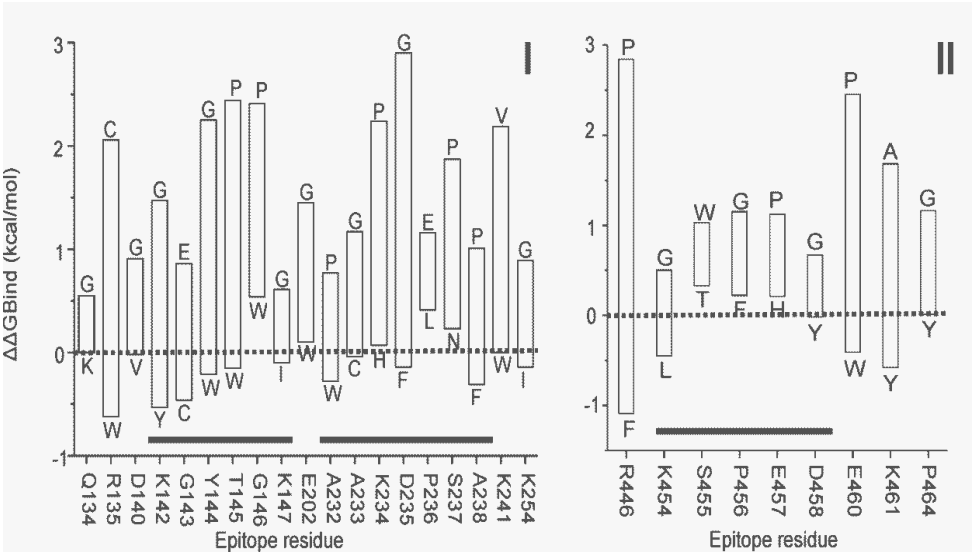

Figure 4: I: Relative binding energy changes between the monoclonal antibody 11H3 and murine GPI upon site-specific exchange of amino acid residues. II: Relative binding energy changes between the monoclonal antibody 46H9 and murine GPI upon site-specific exchange of amino acid residues. Wild-type amino acid residues of the predicted epitope regions are shown at the bottom and are set to 0 kcal/mol (dotted line). Vertical bars show the ΔG_{bind} binding energy ranges after point mutations. Mutated amino acid residues with the highest and the lowest $\Delta\Delta G_{bind}$ values are represented above and below their respective bars for each epitope residue position. The horizontal lines (bold print) indicate continuous sequence stretches of the epitope amino acid residues.

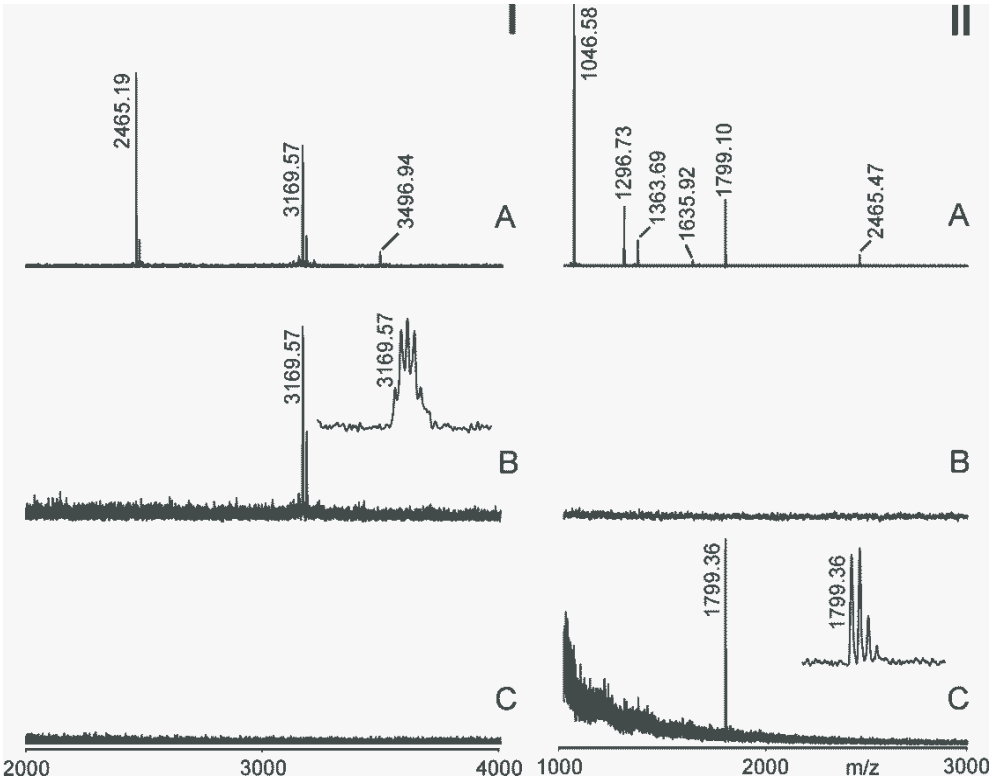

Figure 5: MALDI-TOF mass spectra of peptide mixtures prior to and after epitope extraction. IA: Peptide mixture I. IB: Eluted peptides after epitope extraction using GPI-specific monoclonal antibody 11H3. The insert zooms into the monoisotopic pattern. IC: Eluted solution after exposing peptide mixture I to the 46H9 antibody (non-specific control). For mass assignments of the 11H3 epitope extraction see table S23. IIA: Peptide mixture II. IIB: Eluted solution after exposure of peptide mixture II to the 11H3 antibody (non-specific control). IIC: Eluted peptides after epitope extraction using GPI-specific monoclonal antibody 46H9. The insert zooms into the monoisotopic pattern. For mass assignments of the 46H9 epitope extraction see table S24. Ion signals are labelled. DHB was used as matrix.

after exposure of peptide mixture I to monoclonal antibody 46H9 showed just baseline (Figure 5IC). None of the peptides in mixture I underwent strong interactions to this antibody.

The epitope confirmation of GPI-specific monoclonal antibody 46H9 on murine GPI antigen was performed by affinity mass spectrometry using peptide mixture II (Supplemental Table 24) which consisted of five peptides spreading over the mass range of 1000 Da to 2500 Da. MALDI-ToF MS analysis of peptide mixture II showed singly charged ion signals of the 46H9 epitope peptide and the standard peptides (Figure 5IIA).

Peptide mixture II was then allowed to interact with the GPI-specific monoclonal antibody 46H9 as well as with the monoclonal antibody 11H3, which was used as non-specific control. MALDI-ToF MS analysis of the eluted solution from the exposure of the peptide mixture to 11H3 showed the absence of peptide ion signals (Figure 5IIB), i.e., no binding. By contrast, when peptide mixture II was exposed to 46H9, MALDI-ToF MS analysis (Figure 5IIC) of the eluted solution showed the presence of just one intense singly charged ion signal at m/z 1799.10 which corresponds to the 46H9 epitope peptide. Hence, the experimental results stand in full agreement with the *in silico* predicted GPI epitopes.

Discussion

Since the recombinant GPI antigen is insoluble in non-denaturing buffers, computational prediction methods had to be chosen to approach the determination of the epitopes of the monoclonal antibodies 11H3 and 46H9. Predictions were verified with mass spectrometry-based epitope extraction [51,62,63] using synthetic peptides. The computational tools used for our predictions include the online Rosetta antibody server [39,56] for antibody modeling, and the ClusPro 2.0 server [57] for docking analyses. These computational tools were developed using many data sets and acceptable computational benchmarks.

Of note, due to the large size of our proteins (1336 amino acid residues for the complex between GPI dimer and 46H9 antibody and 1347 amino acid residues for the complex between GPI dimer and 11H3 antibody), *in silico* mutations were performed on all the interfacial residues between the antigen (epitope) and antibody (paratope) complex using a simple, fast, and accurate tool, which depends on a set of statistical potentials derived from known protein structures [50,64] instead of using molecular mechanics/generalized Born surface area calculations (MM-GBSA) [65] and computational alanine scanning [66]. The epitopes of either the 11H3 or the 46H9 monoclonal antibodies on GPI contain surface-exposed loop regions, which is consistent with typical epitope features, such as being surface exposed [67], protruding from the surface of the antigen [68], and occurring in loops [69]. In addition, the presence of loop regions in our predicted epitopes agrees with the notion that protein-protein binding sites often occur at flexible protein regions [70].

Epitope determination, as performed by us, is important for understanding specific biological processes such as the recognition motifs involved in the disease initiation process. For example, biological activity of human CD20 monoclonal antibodies is linked to the unique epitopes on CD20 [71]. It has also been demonstrated that spatial arrangements of the secondary structural elements in epitope II on the hepatitis C virus E2 protein can determine how its specific antibody binds and ultimately directs the outcomes of either antibody-mediated neutralization or non-neutralization [59]. The murine GPI antigen dimer structure extends from left to right by ~8.0 nm and from top to bottom by ~7.8 nm. Since the diameter of the Fab fragment of an antibody is normally between 1.6 nm and 2.3 nm [72], the murine GPI antigen provides sufficient area for simultaneous binding of two and even more GPI-specific monoclonal antibodies (Figure 6).

The GPI dimer can form multimeric complexes with the GPI-specific monoclonal antibodies 11H3 and 46H9, and can appear as an opsonized antigen on the cartilage surface, cross-linking multiple Fragment Crystallizable Receptors (FcR) on cell surfaces, e.g. on macrophages. Such cross-linking events are necessary for the initiation of an inflammatory cascade [12,73]. On intact macrophage cells, FcR clusters with different sizes have been found using high-resolution Atomic Force Microscope (AFM) topography imaging with single-molecule force spectroscopy [74]. The largest FcR clusters were greater than 200 nm in diameter (equivalent to ~15-50 FcRs), whereas smaller

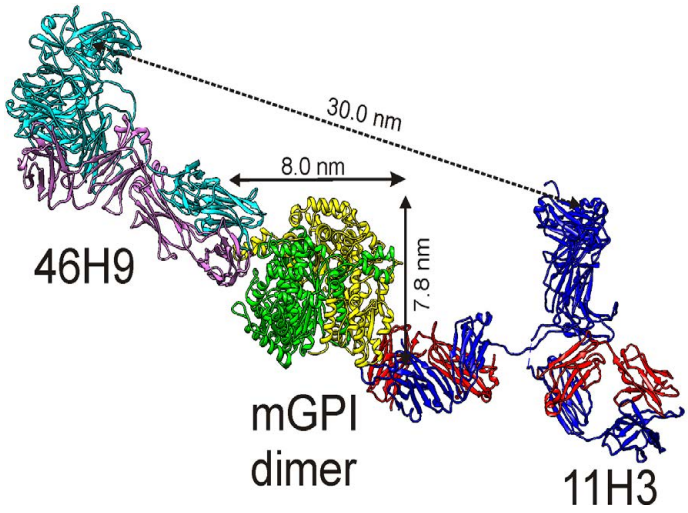

Figure 6: Cartoon view of the immune complex. A murine GPI dimer (yellow and green for A- and B-chain) is simultaneously decorated with GPI-specific monoclonal antibodies 46H9 (left) and 11H3 (right), showing the molecular dimensions of the antigen-antibody complexes. Red and violet: light chains. Blue and cyan: Heavy chains. The molecular dimensions of GPI are given (solid lines) and the distance of the Fc parts of the antibodies is indicated (dotted line).

clusters (micro-domains) were of 60-150 nm (equivalent to ~13-38 FcRs) in size. Since macrophages have a diameter of 40-50 μm it can be estimated that one cell displays ~3,000 to 10,000 FcRs on its surface. The measured distance between the Fc parts of the two GPI-specific monoclonal antibodies 11H3 and 46H9 bound to natively folded murine GPI (Figure 6) is 30 nm and that of the Fc parts bound to completely unfolded (denatured) murine GPI is ~65 nm. In either case (native or denatured GPI) these distances are within the ranges that had been found for FcR distances of intact macrophages. Such compact clustering of the estimated FcRs on the surface of a macrophage cell likely will lead to either phagocytosis of murine GPI antigen-antiGPI antibody immune complexes and/or to the release of lytic enzymes and prostaglandins, which can initiate inflammation and, ultimately, lead to the destruction of cartilage matrix [75]. Additionally, the Fc part of the anti-GPI antibody, when bound to the GPI antigen, is able to covalently bind with the C3b complement protein, which is necessary to activate the alternative complement pathway. Complement protein C5a, resulting from this activation, interacts with C5a receptors which are expressed on neutrophils, macrophages and mast cells [76]. This process leads to production of pro-inflammatory cytokines, such as TNFα and IL-1 and also leads to the destruction of the joints [77]. Recently reported, transfer of monoclonal Anti-Citrullinated Protein/Peptide Antibodies (ACPAs) into Balb/c mice also induced bone loss that was completely reversed by the IL-8 antagonist reparixin [78]. From this study, IL-8 has been identified as a chemokine-dependent molecular mechanism underlying Rheumatoid Arthritis-associated autoantibody-mediated bone loss.

Epitope determination of the pathogenic GPI-specific monoclonal antibodies on the GPI autoantigen eventually leads to the synthesis of epitope-derived peptides that may be used for improved disease diagnosis using peptide-based diagnostic techniques [79]. Epitope-derived peptides can also be envisaged to find use as vaccines for patient therapy, as demonstrated in cancer treatment [80]. The epitope peptides will also be useful for generating anti-anti-GPI-specific anti-idiotypic antibodies from IVIg preparations [81], which can be used for treatment of arthritis in the K/BxN mouse model and subsequently for targeting GPI-specific autoantibodies in RA patients. Knowledge of the epitopes of GPI-specific monoclonal antibodies 11H3 and 46H9 paves the way for understanding the principle of function for disease onset processes in the K/BxN mouse disease at the molecular level.

Author's Contributions

MOG conceived the study and coordinated the work and manuscript writing. KFMO, MOG and PCA designed, analyzed and interpreted epitope prediction work. SS, FM, DF and HI generated the disease initiating monoclonal antibodies 11H3 and 46H9 and performed DNA sequencing of the antibodies. KFMO, CK and CR performed and analyzed the epitope mapping experiments. KFMO, CK, CR, MOG, HI and PCA wrote the manuscript. All authors reviewed and approved the final version of the manuscript.

Acknowledgments

We would like to acknowledge Dr. Stefan Mikkat and Ms. Manuela Ruß for their expertise on mass spectrometry. KFMO was supported financially by Hermes grant (HP 002/2014)-University of Rostock, University of Washington Bothell and by the German Academic Exchange Service (DAAD) (91548123).

References

1. Feldmann M, Brennan FM, Maini RN (1996) Rheumatoid arthritis. Cell 85: 307-310.
2. Glocker MO, Guthke R, Kekow J, Thiesen HJ (2006) Rheumatoid arthritis, a complex multifactorial disease: on the way toward individualized medicine. Med Res Rev 26: 63-87.
3. Davidson A, Diamond B (2001) Autoimmune diseases. N Eng J Med 345: 340-350.
4. Cha HS, Kim TJ, Kim JY, Lee MH, Jeon CH, et al. (2004) Autoantibodies to glucose-6-phosphate isomerase are elevated in the synovial fluid of rheumatoid arthritis patients. Scand J Rheumatol 33: 179-184.
5. Fan LY, Zong M, Wang Q, Yang L, Sun LS, et al. (2010) Diagnostic value of glucose-6-phosphate isomerase in rheumatoid arthritis. Clin Chim Acta 411: 2049-2053.
6. Kassahn D, Kolb C, Solomon S, Bochtler P, Illges H (2002) Few human autoimmune sera detect GPI. Nat Immunol 3: 411-412.
7. Monach PA, Mathis D, Benoist C (2001) The K/BxN Arthritis Model. Curr Protoc Immunol.
8. Korganow AS, Ji H, Mangialaio S, Duchatelle V, Pelanda R, et al. (1999) From systemic T cell self-reactivity to organ-specific autoimmune disease via immunoglobulins. Immunity 10: 451-461.
9. Kouskoff V, Korganow AS, Duchatelle V, Degott C, Benoist C, et al. (1996) Organ-specific disease provoked by systemic autoimmunity. Cell 87: 811-822.
10. Matsumoto I, Maccioni M, Lee DM, Maurice M, Simmons B, et al. (2002) How antibodies to a ubiquitous cytoplasmic enzyme may provoke joint-specific autoimmune disease. Nat Immunol 3: 360-365.
11. Wipke BT, Wang Z, Kim J, McCarthy TJ, Allen PM (2002) Dynamic visualization of a joint-specific autoimmune response through positron emission tomography. Nat Immunol 3: 366-372.
12. Maccioni M, Zeder-Lutz G, Huang H, Ebel C, Gerber P, et al. (2002) Arthritogenic monoclonal antibodies from K/BxN mice. J Exp Med 195: 1071-1077.
13. Solomon S (2003) Role of pathogenic auto-antibodies and innate immunity mediators in K/BxN murine model for rheumatoid arthritis [Thesis]: University of Konstanz, Germany.
14. He L, Zhu J (2015) Computational tools for epitope vaccine design and evaluation. Curr Opin Virol 11: 103-112.
15. Sela-Culang I, Ofran Y, Peters B (2015) Antibody specific epitope prediction-emergence of a new paradigm. Curr Opin Virol 11: 98-102.
16. Yao B, Zheng D, Liang S, Zhang C (2013) Conformational B-cell epitope prediction on antigen protein structures: a review of current algorithms and comparison with common binding site prediction methods. PLoS ONE 8: e62249.
17. Ponomarenko JV, van Regenmortel MHV (2009) B-Cell Epitope Prediction. In: Gu J, Bourne PE, editors. Structural Bioinformatics (2nd edn.). John Wiley & Sons, Inc., Hoboken, NJ, USA.
18. Morris GE (2008) Epitope mapping. Identification of Antibody-Binding Sites on Protein Antigens. In: Walker JM, Rapley R, editors. Molecular Biomethods Handbook. 2nd ed. Humana Press, Totowa, NJ.
19. Opuni KF, Al-Majdoub M, Yefremova Y, El-Kased RF, Koy C, et al. (2016) Mass spectrometric epitope mapping. Mass Spectrom Rev 9999: 1-13.
20. Suckau D, Kohl J, Karwath G, Schneider K, Casaretto M, et al. (1990) Molecular epitope identification by limited proteolysis of an immobilized antigen-antibody complex and mass spectrometric peptide mapping. Proc Natl Acad Sci USA 87: 9848-9852.
21. Macht M, Fiedler W, Kurzinger K, Przybylski M (1996) Mass spectrometric mapping of protein epitope structures of myocardial infarct markers myoglobin and troponin T. Biochemistry 35: 15633-15639.
22. Clementi N, Mancini N, Castelli M, Clementi M, Burioni R (2013) Characterization of epitopes recognized by monoclonal antibodies: experimental approaches supported by freely accessible bioinformatic tools. Drug Discov Today 18: 464-471.
23. Kringelum JV, Nielsen M, Padkjaer SB, Lund O (2013) Structural analysis of B-cell epitopes in antibody:protein complexes. Mol Immunol 53: 24-34.
24. El-Manzalawy Y, Honavar V (2010) Recent advances in B-cell epitope prediction methods. Immunome Res 6: S2.
25. Gao J, Kurgan L (2014) Computational prediction of B cell epitopes from antigen sequences. Methods Mol Biol 1184: 197-215.

26. Greenbaum JA, Andersen PH, Blythe M, Bui HH, Cachau RE, et al. (2007) Towards a consensus on datasets and evaluation metrics for developing B-cell epitope prediction tools. J Mol Recognit 20: 75-82.

27. Kringelum JV, Lundegaard C, Lund O, Nielsen M (2012) Reliable B cell epitope predictions: impacts of method development and improved benchmarking. PLoS Comput Biol 8: e1002829.

28. Ponomarenko JV, Bourne PE (2007) Antibody-protein interactions: benchmark datasets and prediction tools evaluation. BMC Struct Biol 7: 64.

29. Soria-Guerra RE, Nieto-Gomez R, Govea-Alonso DO, Rosales-Mendoza S (2015) An overview of bioinformatics tools for epitope prediction: implications on vaccine development. J Biomed Inform 53: 405-414.

30. Sun P, Ju H, Liu Z, Ning Q, Zhang J, et al. (2013) Bioinformatics resources and tools for conformational B-cell epitope prediction. Comput Math Methods Med 2013: 943636.

31. Yang X, Yu X (2009) An introduction to epitope prediction methods and software. Rev Med Virol 19: 77-96.

32. Zhang W, Niu Y, Xiong Y, Ke M (2014) Prediction of conformational B-cell epitopes. Methods Mol Biol 1184: 185-196.

33. Caoili SEC (2010) B-cell epitope prediction for peptide-based vaccine design: towards a paradigm of biological outcomes. Proceedings of the First ACM International Conference on Bioinformatics and Computational Biology. Niagara Falls, NY, USA pp: 602-610.

34. Lassaux P, Peri C, Ferrer-Navarro M, Gourlay LJ, Gori A, et al. (2013) A structure-based strategy for epitope discovery in Burkholderia pseudomallei OppA antigen. Structure 21: 167-175.

35. Tambunan US, Sipahutar FR, Parikesit AA, Kerami D (2016) Vaccine Design for H5N1 Based on B- and T-cell Epitope Predictions. Bioinform Biol Insights 10: 27-35.

36. Solomon S, Kolb C, Mohanty S, Jeisy-Walder E, Preyer R, et al. (2002) Transmission of antibody-induced arthritis is independent of complement component 4 (C4) and the complement receptors 1 and 2 (CD21/35). Euro J Immunol 32: 644-651.

37. Lefranc MP, Giudicelli V, Kaas Q, Duprat E, Jabado-Michaloud J, et al. (2005) IMGT, the international ImMunoGeneTics information system. Nucleic Acids Res 33: D593-D597.

38. Lyskov S, Chou FC, Conchuir SO, Der BS, Drew K, et al. (2013) Serverification of molecular modeling applications: the Rosetta Online Server that Includes Everyone (ROSIE). PLoS ONE 8: e63906.

39. Sivasubramanian A, Sircar A, Chaudhury S, Gray JJ (2009) Toward high-resolution homology modeling of antibody Fv regions and application to antibody-antigen docking. Proteins 74: 497-514.

40. Pettersen EF, Goddard TD, Huang CC, Couch GS, Greenblatt DM, et al. (2004) UCSF Chimera–a visualization system for exploratory research and analysis. J Comput Chem 25: 1605-1612.

41. Kozakov D, Beglov D, Bohnuud T, Mottarella SE, Xia B, et al. (2013) How good is automated protein docking? Proteins 81: 2159-2166.

42. Lensink MF, Wodak SJ (2013) Docking, scoring, and affinity prediction in CAPRI. Proteins 81: 2082-2095.

43. Linnebacher M, Lorenz P, Koy C, Jahnke A, Born N, et al. (2012) Clonality characterization of natural epitope-specific antibodies against the tumor-related antigen topoisomerase IIa by peptide chip and proteome analysis: a pilot study with colorectal carcinoma patient samples. Anal Bioanal Chem 403: 227-238.

44. Van Der Spoel D, Lindahl E, Hess B, Groenhof G, Mark AE, et al. (2005) GROMACS: fast, flexible, and free. J Comput Chem 26: 1701-1718.

45. Lindorff-Larsen K, Piana S, Palmo K, Maragakis P, Klepeis JL, et al. (2010) Improved side-chain torsion potentials for the Amber ff99SB protein force field. Proteins 78: 1950-1958.

46. Jorgensen WL, Jayaraman C, Madura JD, Impey RW, Klein ML (1983) Comparison of simple potential functions for simulating liquid water. J Chem Phys 79: 926-935.

47. Berendsen HJC, Postma JPM, van Gunsteren WF, DiNola A, Haak JR (1984) Molecular dynamics with coupling to an external bath. J Chem Phys 81: 3684-3690.

48. Essmann U, Perera L, Berkowitz ML (1995) A smooth particle mesh Ewald method. J Chem Phys 103: 8577-8593.

49. Hess B, Bekker H, Berendsen HJC, Fraaije JGEM (1997) LINCS: A linear constraint solver for molecular simulations. J Comput Chem 18: 1463-1472.

50. Dehouck Y, Kwasigroch JM, Rooman M, Gilis D (2013) BeAtMuSiC: Prediction of changes in protein-protein binding affinity on mutations. Nucleic Acids Res 41: W333-W3399.

51. Al-Majdoub M, Opuni KF, Koy C, Glocker MO (2013) Facile fabrication and instant application of miniaturized antibody-decorated affinity columns for higher-order structure and functional characterization of TRIM21 epitope peptides. Anal Chem 85: 10479-10487.

52. Sinz A, Bantscheff M, Mikkat S, Ringel B, Drynda S, et al. (2002) Mass spectrometric proteome analyses of synovial fluids and plasmas from patients suffering from rheumatoid arthritis and comparison to reactive arthritis or osteoarthritis. Electrophoresis 23: 3445-3456.

53. Al-Majdoub M, Koy C, Lorenz P, Thiesen HJ, Glocker MO (2013) Mass spectrometric and peptide chip characterization of an assembled epitope: analysis of a polyclonal antibody model serum directed against the Sjogren/systemic lupus erythematosus autoantigen TRIM21. J Mass Spectrom 48: 651-659.

54. Gray JJ, Moughon SE, Kortemme T, Schueler-Furman O, Misura KM, et al. (2003) Protein-protein docking predictions for the CAPRI experiment. Proteins 52: 118-122.

55. Al-Lazikani B, Lesk AM, Chothia C (1997) Standard conformations for the canonical structures of immunoglobulins. J Mol Biol 273: 927-948.

56. Sircar A, Kim ET, Gray JJ (2009) RosettaAntibody: antibody variable region homology modeling server. Nucleic Acids Res 37: W474-W479.

57. Brenke R, Hall DR, Chuang GY, Comeau SR, Bohnuud T, et al. (2012) Application of asymmetric statistical potentials to antibody-protein docking. Bioinformatics 28: 2608-2614.

58. Rubinstein ND, Mayrose I, Halperin D, Yekutieli D, Gershoni JM, et al. (2008) Computational characterization of B-cell epitopes. Mol Immunol 45: 3477-3489.

59. Deng L, Ma L, Virata-Theimer ML, Zhong L, Yan H, et al. (2014) Discrete conformations of epitope II on the hepatitis C virus E2 protein for antibody-mediated neutralization and nonneutralization. Proc Natl Acad Sci U S A 111: 10690-10695.

60. Gutierrez LJ, Andujar SA, Enriz RD, Baldoni HA (2014) Structural and functional insights into the anti-BACE1 Fab fragment that recognizes the BACE1 exosite. J Biomol Struct Dyn 32: 1421-1433.

61. Tina KG, Bhadra R, Srinivasan N (2007) PIC: Protein Interactions Calculator. Nucleic Acids Res 35: W473-W476.

62. Al-Majdoub M, Opuni KF, Yefremova Y, Koy C, Lorenz P, et al. (2014) A novel strategy for the rapid preparation and isolation of intact immune complexes from peptide mixtures. J Mol Recognit 27: 566-574.

63. Rathore RS, Sumakanth M, Reddy MS, Reddanna P, Rao AA, et al. (2013) Advances in binding free energies calculations: QM/MM-based free energy perturbation method for drug design. Curr Pharm Des 19: 4674-4686.

64. Moretti R, Fleishman SJ, Agius R, Torchala M, Bates PA, et al. (2013) Community-wide evaluation of methods for predicting the effect of mutations on protein-protein interactions. Proteins 81: 1980-1987.

65. Gilson MK, Zhou HX (2007) Calculation of protein-ligand binding affinities. Annu Rev Biophys Biomol Struct 36: 21-42.

66. Kortemme T, Kim DE, Baker D (2004) Computational alanine scanning of protein-protein interfaces. Sci STKE 219: pl2.

67. Novotny J, Handschumacher M, Haber E, Bruccoleri RE, Carlson WB, et al. (1986) Antigenic determinants in proteins coincide with surface regions accessible to large probes (antibody domains). Proc Natl Acad Sci USA 83: 226-230.

68. Thornton JM, Edwards MS, Taylor WR, Barlow DJ (1986) Location of 'continuous' antigenic determinants in the protruding regions of proteins. EMBO J 5: 409-413.

69. El-Kased RF, Koy C, Deierling T, Lorenz P, Qian Z, et al. (2009) Mass spectrometric and peptide chip epitope mapping of rheumatoid arthritis autoantigen RA33. Eur J Mass Spectrom (Chichester, Eng) 15: 747-759.

70. Neuvirth H, Raz R, Schreiber G (2004) ProMate: a structure based prediction program to identify the location of protein-protein binding sites. J Mol Biol 338: 181-199.

71. Teeling JL, Mackus WJ, Wiegman LJ, van den Brakel JH, Beers SA, et al. (2006) The biological activity of human CD20 monoclonal antibodies is linked to unique epitopes on CD20. J Immunol 177: 362-371.

72. Guddat LW, Herron JN, Edmundson AB (1993) Three-dimensional structure of a human immunoglobulin with a hinge deletion. Proc Natl Acad Sci USA 90: 4271-4275.

73. Solomon S, Kassahn D, Illges H (2005) The role of the complement and the Fc gamma R system in the pathogenesis of arthritis. Arthritis Res Ther 7: 129-135.

74. Ahmad SF, Chtcheglova LA, Mayer B, Kuznetsov SA, Hinterdorfer P (2011) Nanosensing of Fcgamma receptors on macrophages. Anal Bioanal Chem 399: 2359-2367.

75. Solomon S, Rajasekaran N, Jeisy-Walder E, Snapper SB, Illges H (2005) A crucial role for macrophages in the pathology of K/B x N serum-induced arthritis. Eur J Immunol 35: 3064-3073.

76. Ji H, Ohmura K, Mahmood U, Lee DM, Hofhuis FM, et al. (2002) Arthritis critically dependent on innate immune system players. Immunity 16: 157-168.

77. Feldmann M, Brennan FM, Maini RN (1996) Role of cytokines in rheumatoid arthritis. Annu Rev Immunol 14: 397-440.

78. Krishnamurthy A, Joshua V, Haj Hensvold A, Jin T, Sun M, et al. (2016) Identification of a novel chemokine-dependent molecular mechanism underlying rheumatoid arthritis-associated autoantibody-mediated bone loss. Ann Rheum Dis 75: 721-729.

79. Klareskog L, Ronnelid J, Lundberg K, Padyukov L, Alfredsson L (2008) Immunity to citrullinated proteins in rheumatoid arthritis. Annu Rev Immunol 26: 651-675.

80. Slingluff CL Jr, Petroni GR, Olson W, Czarkowski A, Grosh WW, et al. (2008) Helper T-cell responses and clinical activity of a melanoma vaccine with multiple peptides from MAGE and melanocytic differentiation antigens. J Clin Oncol 26: 4973-4980.

81. Svetlicky N, Kivity S, Odeh Q, Shovman O, Gertel S, et al. (2015) Anti-citrullinated-protein-antibody-specific intravenous immunoglobulin attenuates collagen-induced arthritis in mice. Clin Exp Immunol 182: 241-250.